Neonatal ghrelin programs development of hypothalamic feeding circuits

Sophie M. Steculorum, … , Sven Klussmann, Sebastien G. Bouret

Research Article

A complex neural network regulates body weight and energy balance, and dysfunction in the communication between the gut and this neural network is associated with metabolic diseases, such as obesity. The stomach-derived hormone ghrelin stimulates appetite through interactions with neurons in the arcuate nucleus of the hypothalamus (ARH). Here, we evaluated the physiological and neurobiological contribution of ghrelin during development by specifically blocking ghrelin action during early postnatal development in mice. Ghrelin blockade in neonatal mice resulted in enhanced ARH neural projections and long-term metabolic effects, including increased body weight, visceral fat, and blood glucose levels and decreased leptin sensitivity. In addition, chronic administration of ghrelin during postnatal life impaired the normal development of ARH projections and caused metabolic dysfunction. Consistent with these observations, direct exposure of postnatal ARH neuronal explants to ghrelin blunted axonal growth and blocked the neurotrophic effect of the adipocyte-derived hormone leptin. Moreover, chronic ghrelin exposure in neonatal mice also attenuated leptin-induced STAT3 signaling in ARH neurons. Collectively, these data reveal that ghrelin plays an inhibitory role in the development of hypothalamic neural circuits and suggest that proper expression of ghrelin during neonatal life is pivotal for lifelong metabolic regulation.

Find the latest version:

https://jci.me/73688/pdf

Neonatal ghrelin programs development of hypothalamic feeding circuits

Sophie M. Steculorum,[1,2] Gustav Collden,[2] Berengere Coupe,[1] Sophie Croizier,[1,2] Sarah Lockie,[3] Zane B. Andrews,[3] Florian Jarosch,[4] Sven Klussmann,[4] and Sebastien G. Bouret[1,2]

[1]The Saban Research Institute, Developmental Neuroscience Program, Children's Hospital Los Angeles, University of Southern California, Los Angeles, California, USA. [2]Inserm, Jean-Pierre Aubert Research Center, U1172, University Lille 2, Lille, France. [3]Department of Physiology, Monash University, Clayton, Victoria, Australia. [4]NOXXON Pharma AG, Berlin, Germany.

A complex neural network regulates body weight and energy balance, and dysfunction in the communication between the gut and this neural network is associated with metabolic diseases, such as obesity. The stomach-derived hormone ghrelin stimulates appetite through interactions with neurons in the arcuate nucleus of the hypothalamus (ARH). Here, we evaluated the physiological and neurobiological contribution of ghrelin during development by specifically blocking ghrelin action during early postnatal development in mice. Ghrelin blockade in neonatal mice resulted in enhanced ARH neural projections and long-term metabolic effects, including increased body weight, visceral fat, and blood glucose levels and decreased leptin sensitivity. In addition, chronic administration of ghrelin during postnatal life impaired the normal development of ARH projections and caused metabolic dysfunction. Consistent with these observations, direct exposure of postnatal ARH neuronal explants to ghrelin blunted axonal growth and blocked the neurotrophic effect of the adipocyte-derived hormone leptin. Moreover, chronic ghrelin exposure in neonatal mice also attenuated leptin-induced STAT3 signaling in ARH neurons. Collectively, these data reveal that ghrelin plays an inhibitory role in the development of hypothalamic neural circuits and suggest that proper expression of ghrelin during neonatal life is pivotal for lifelong metabolic regulation.

Introduction

In the midst of the present obesity epidemic, there is a need to better understand the mechanisms and factors involved in the development of this pathological condition. The physiological mechanisms that underlie hunger and satiety have only recently been determined (1, 2). The discovery of leptin and ghrelin led to a paradigm shift in our understanding with the realization that our subconscious motivation to eat can be powerfully and dynamically regulated by hormonal signals (3–5). Epidemiological studies and animal models have provided valuable information on the role of the perinatal environment in the susceptibility for diseases in adult life, such as obesity and type 2 diabetes. Previous studies showed that various environmental challenges, including deficient or excess nutrition, during development program organisms for metabolic diseases in later life (6–8).

Body weight and energy balance are dynamically regulated by a sophisticated network of neural circuits. At the center of this regulatory network is the arcuate nucleus of the hypothalamus (ARH), which contains sets of neurons devoted to metabolic regulation. The ARH comprises orexigenic neurons that coproduce neuropeptide Y (NPY) and agouti-related peptide (AgRP) as well as anorexigenic neurons that contain proopiomelanocortin-derived (POMC-derived) peptides. These ARH neuronal populations are directly regulated by leptin and ghrelin (9, 10). NPY/AgRP and POMC neurons provide overlapping projections to other parts of the hypothalamus, including the paraventricular nucleus of the hypothalamus (PVH) and the dorsomedial nucleus of the hypothalamus (DMH) and the lateral hypothalamic area (LHA), to exert their metabolic effects (11, 12).

It has been suggested that impaired hypothalamic development during perinatal life results in lifelong metabolic dysregulation because of the importance of the hypothalamus in the control of eating and energy balance (6). In mice, ARH neural projections primarily develop during the first 3 weeks of postnatal life under the influence of genetic and environmental factors, including endocrine signals (8, 13). Leptin represents a powerful neurotrophic agent that promotes the formation of ARH-derived circuits (14). However, the exact nature of hormonal factors that influence the development of appetite-related neural projections remains elusive and mainly restricted to the well-described axonotrophic effect of leptin (14). For example, little is known about the biological function of ghrelin during neonatal life. However, despite the well-documented orexigenic effect of ghrelin, the congenital deletion of ghrelin or its receptors results in normal body weight, growth rate, and food intake (15–18), raising the possibility that lack of ghrelin during early life may cause compensatory developmental changes (19). The observation that maternal ghrelin injection causes high birth weight in the offspring also supports a role for neonatal ghrelin in growth and development (20).
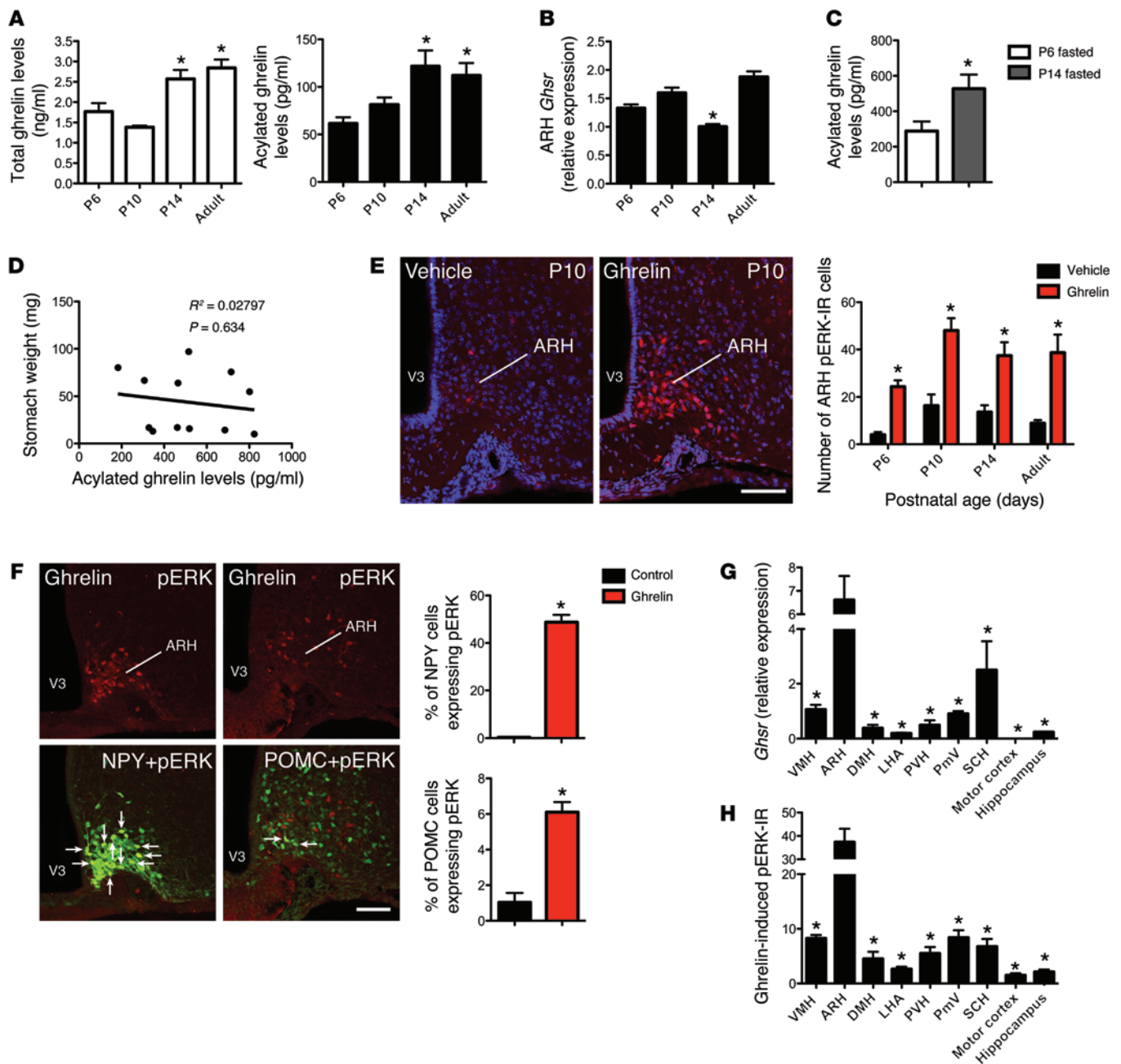
Figure 1. Ghrelin signaling in neonatal ARH neurons. (**A**) Total plasma ghrelin levels and acylated ghrelin levels of P6, P10, P14, and adult mice ($n = 6$ for P10; $n = 5$ for P6 and P14; $n = 4$ for adult). (**B**) Relative expression of *Ghsr* mRNA in the ARH of P6, P10, P14, and adult mice ($n = 6$ for P10; $n = 5$ for P6 and P14; $n = 4$ for adult). (**C**) Circulating acylated ghrelin levels of P6 and P14 mice after a 4-hour fasting ($n = 6$ per group). (**D**) Correlation between stomach weight and circulating acylated ghrelin levels in P14 mice ($n = 12$ per group). (**E**) Confocal images and quantitative comparisons of pERK+ cells after administration of ghrelin or vehicle alone in P6, P10, P14, and adult mice ($n = 5$ for P10 and P14; $n = 4$ for P6 and adult). (**F**) Confocal images and quantitative comparisons of pERK+ cells after administration of ghrelin or vehicle alone in NPY- and POMC-GFP pups on P10 ($n = 4$ for vehicle; $n = 5$ for ghrelin). Arrows point to double-labeled cells. (**G**) Relative expression of *Ghsr* mRNA in the brains of P14 mice ($n = 4$ per group). (**H**) Quantitative comparisons of pERK+ cells in the brains of P14 mice after administration of ghrelin ($n = 4$). Values are shown as the mean ± SEM. PmV, ventral premammillary nucleus; SCH, suprachiasmatic nucleus; VMH, ventromedial nucleus; V3, third ventricle. *$P < 0.05$ vs. P6 and P10 (**A**); vs. P6, P10, and adult (**B**); vs. P6 fasted (**C**); vs. vehicle (**E** and **F**); and vs. ARH (**G** and **H**). Statistical significance was determined using 2-tailed Student's *t* tests (**C** and **F**) and a 2-way ANOVA followed by Bonferroni's post-hoc test (**A**, **B**, **E**, **G**, and **H**). Scale bars: 120 μm.

In the present study, we selectively inhibited the action of ghrelin during the preweaning period to determine the role of neonatal ghrelin in hypothalamic development and adult metabolic regulation. We also investigated whether abnormally elevated levels of ghrelin, during a developmental period when endogenous ghrelin levels are low, have enduring effects on hypothalamic development and metabolic regulation. The results indicate that neonatal ghrelin is important for normal maturation of hypothalamic axonal projections, and that the perturbation in ghrelin action during the preweaning period results in lifelong metabolic disturbances.
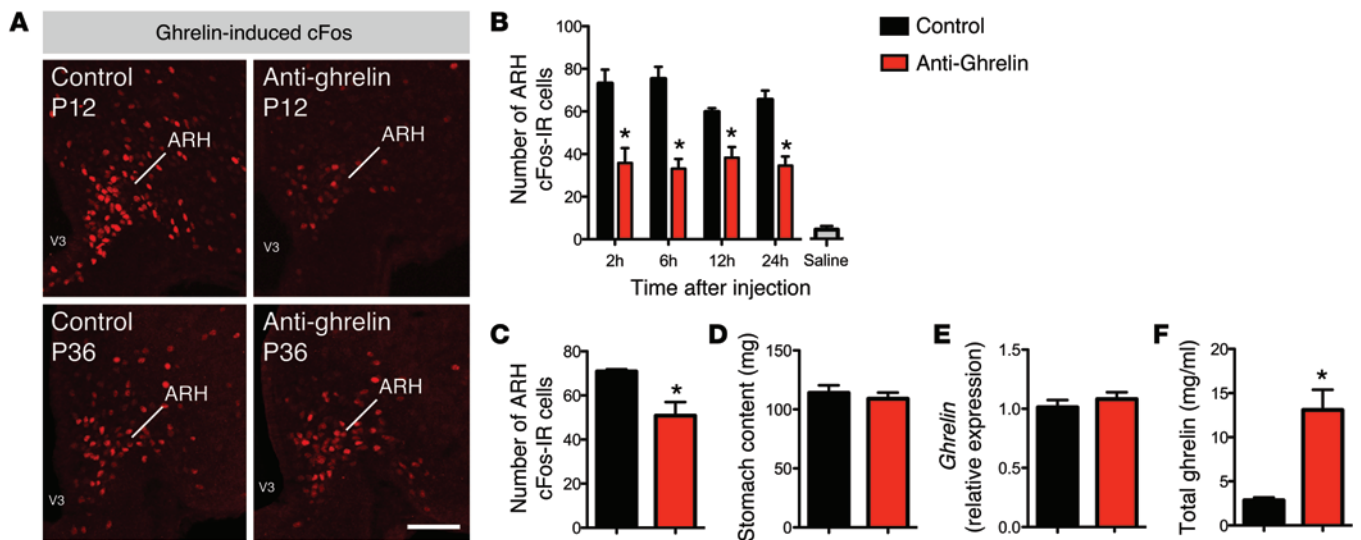
Figure 2. Effects of the anti-ghrelin compound. (**A**) Representative images of ghrelin-induced cFos IR (marker of cellular activation) from P12 and P36 mice neonatally injected with control or anti-ghrelin. (**B**) Quantitative comparisons of ghrelin-induced cFos IR in the ARH of P12 mice 2, 6, 12, and 24 hours after i.p. administration of control or anti-ghrelin ($n = 3$ for control; $n = 4$ for saline and anti-ghrelin). The gray bar shows the number of cFos-IR cells in saline-treated animals. (**C**) Number of cFos-IR cells of P21 mice neonatally injected with control or anti-ghrelin 2 hours after i.p. administration of ghrelin (2 mg/kg) ($n = 3$ per group). (**D**) Stomach content of P14 pups injected with the control or anti-ghrelin compound ($n = 7$ for control; $n = 8$ for anti-ghrelin). (**E**) Relative expression of *ghrelin* mRNA in the stomachs of P14 pups injected with control or anti-ghrelin ($n = 7$ per group). (**F**) Total plasma ghrelin levels of P14 pups injected with control or anti-ghrelin ($n = 7$ per group). Values are shown as the mean ± SEM. *$P < 0.05$ vs. control. Statistical significance was determined using 2-tailed Student's *t* tests (**C–F**) and a 2-way ANOVA followed by Bonferroni's post-hoc test (**B**). Scale bar: 120 μm.

The data also underline the importance of the correct timing and amplitude in ghrelin's action for normal development of hypothalamic neural circuits.

Results

Ghrelin is developmentally regulated and acts on ARH neurons during early life. To assess the function of neonatal ghrelin, we first examined the levels of circulating ghrelin in neonatal mice. Relatively low levels of total and acylated ghrelin were found in the serum at P6; however, the levels increased after P10 and reached adult-like levels by P14 (Figure 1A). This increase in circulating ghrelin levels between P6 and P14 was also observed in fasted pups (Figure 1C), supporting the hypothesis that these changes in ghrelin levels are developmentally acquired versus the hypothesis that they are caused by changes in nutrition. Consistent with this idea, no correlation was found between stomach weight and acylated ghrelin levels at P14 (Figure 1D). To determine whether neonatal ghrelin acts on the developing hypothalamus, we next examined the mRNA expression of the ghrelin receptor *Ghsr* in the ARH of neonatal mice. The ARH of P6 and P10 neonates contained levels of *Ghsr* mRNA that were similar to those found in adult animals (Figure 1B). However, *Ghsr* mRNA decreased at P14, i.e., when neonatal ghrelin levels are elevated (Figure 1B). Ghrelin acts via multiple intracellular signaling pathways, including the MEK/ERK pathway, to modulate cellular and organismal physiology (21). Accordingly, we used the immunohistochemical detection of phosphorylated (activated) forms of ERK (pERK) to examine the ability of ghrelin to activate GHSR in neonatal ARH neurons. A peripheral injection of ghrelin in WT mice robustly induced pERK immunoreactivity (IR) as early as P6 (Figure 1E), indicating that ghrelin can act on ARH neurons when endogenous levels of this hormone are low. However, there was a 1.5- to 2-fold

increase in the number of pERK-IR cells between P6 and P10–P90 animals (Figure 1E). To explore the potential cell-type specificity of ghrelin's action, we examined the ability of ghrelin to activate ERK in the NPY/AgRP and POMC neurons of neonatal animals. We found ghrelin-stimulated pERK IR colocalized with green fluorescent protein (GFP) in the ARH of P10 transgenic mice expressing GFP in NPY- and POMC-containing neurons (Figure 1F). This analysis revealed that neonatal ghrelin stimulated pERK IR in approximately 60% and 10% of NPY and POMC neurons, respectively. Also, 80% and 8% of pERK-IR cells were NPY[+] and POMC[+], respectively.

Blockade of ghrelin action during early life causes metabolic disturbances. To determine the physiological importance of neonatal ghrelin, we selectively inhibited the action of ghrelin during the preweaning period using NOX-B11-2, an anti-ghrelin compound based on a mirror-image oligonucleotide (so-called Spiegelmer) that specifically binds and inhibits the bioactive acylated form of ghrelin (22). Starting at P4, pups were treated daily with i.p. injections of the anti-ghrelin compound or an inactive control, for a total of 18 days. To confirm that the action of ghrelin was specifically disrupted during the injection period, we first examined ghrelin-induced cFos IR, which is a marker of neuronal activation. Neonates injected with the anti-ghrelin compound had an attenuated response to ghrelin as revealed by a reduced number of cFos-IR cells in the ARH following ghrelin injection (Figure 2A). This reduction in ghrelin-induced cFos IR was observed 2 hours after the anti-ghrelin treatment and persisted for up to 24 hours after the injection (Figure 2B). A significant reduction of ghrelin-induced cFos IR was also observed in pups treated with the anti-ghrelin compound for 18 days (Figure 2C). However, P36 animals treated with the anti-ghrelin compound neonatally displayed a normal central response to ghrelin, which shows that the effect is reversible (Fig-
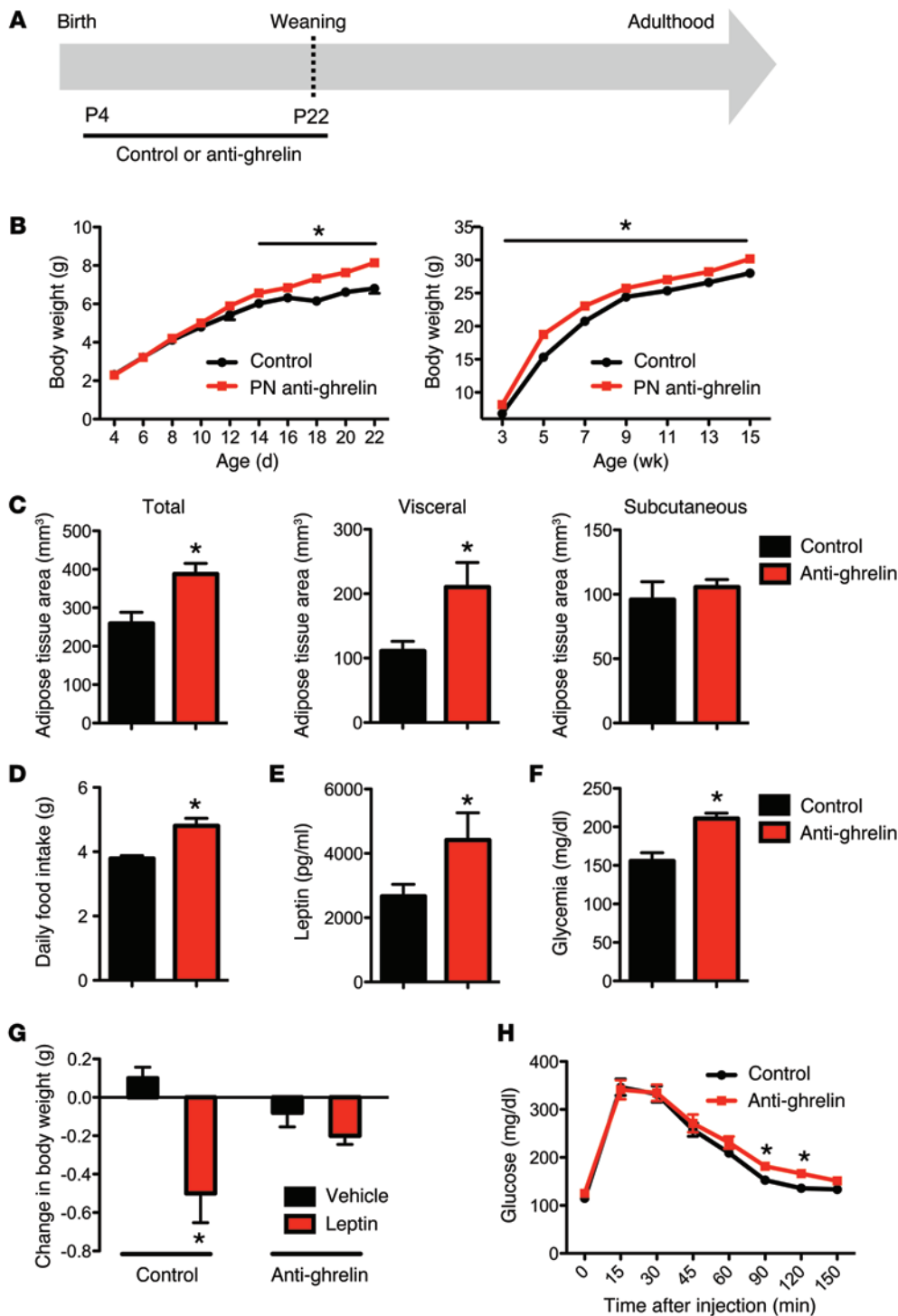
Figure 3. Neonatal ghrelin blockade causes metabolic disturbances. (**A**) Schematic representation of the experimental design used to specifically block ghrelin action during neonatal life. Starting at P4, pups were treated daily with i.p. injections of the anti-ghrelin compound NOX-B11-2 (15 mg/kg) or an inactive control, for a total of 18 days. (**B**) Pre- and post-weaning growth curves (body weights) of mice neonatally injected with control or anti-ghrelin compound (n = 8 for control; n = 10 for anti-ghrelin). (**C**) Body adiposity assessed by MRI at 120 days of age in animals neonatally injected with control or anti-ghrelin (n = 3 for control; n = 4 for anti-ghrelin). (**D**) The daily food intake of P90 mice neonatally injected with control or anti-ghrelin (n = 6 for control; n = 8 for anti-ghrelin). (**E**) Plasma leptin and (**F**) blood glucose levels at 70 days of age in mice neonatally injected with control or anti-ghrelin (n = 6 for control; n = 8 for anti-ghrelin). (**G**) Leptin sensitivity at 100 days of age in mice neonatally injected with control or anti-ghrelin (n = 5 per group). (**H**) Glucose tolerance test of P80–P100 mice neonatally injected with control or anti-ghrelin (n = 12 per group). Values are shown as the mean ± SEM. PN, postnatal. *$P < 0.05$ vs. control or vehicle. Statistical significance was determined using 2-tailed Student's t tests (**C**–**G**) and a 2-way ANOVA followed by Bonferroni's post-hoc test (**B** and **H**).

ure 2A). Notably, the stomach content of the anti-ghrelin–treated neonates appeared similar to that of control animals, suggesting that the anti-ghrelin compound does not alter milk intake (Figure 2D). Stomach *ghrelin* mRNA levels were similar between the anti-ghrelin and control neonates (Figure 2E), but, as previously reported (23), animals treated with the anti-ghrelin compound displayed elevated levels of ghrelin (Figure 2F). This increase in ghrelin levels is expected because the anti-ghrelin compound was modified with a 40-kDa polyethylene glycol, which delayed the elimination of the NOX-B11-2 and the ghrelin–NOX-B11-2 complex.

Physiologically, the anti-ghrelin–injected neonates survived to adulthood and had body weights indistinguishable from those of their control littermates until P14 (Figure 3, A and B). Starting at P14, the anti-ghrelin–treated neonates had significantly higher body weights than the control mice, and they remained overweight after weaning and until adulthood (Figure 3B). Notably, there was no difference in body length between the anti-ghrelin–treated neonates and control mice (data not shown). The daily food intake was significantly higher in adult mice treated with the anti-ghrelin compound neonatally when compared with control mice (Figure

3D). Moreover, adult mice treated with the anti-ghrelin compound neonatally displayed an increase in body fat mass characterized by a higher visceral fat accumulation and an unchanged subcutaneous fat accumulation (Figure 3C). Consistent with these findings, anti-ghrelin–treated mice have elevated levels of leptin (Figure 3E), and altered leptin sensitivity (Figure 3G), when compared with control mice. In addition, the fed glucose levels were significantly elevated in the adult mice treated with the anti-ghrelin compound neonatally (Figure 3F), and anti-ghrelin–treated mice displayed elevated levels of glucose 90–120 minutes after a glucose challenge, as compared with control mice (Figure 3H).

Alteration of ghrelin action during neonatal life affects development of ARH neuronal projections. During development, axonal projections ascend from the ARH to reach their target nuclei, such as the PVH, during the second week of life (14). To investigate whether neonatal ghrelin blockade influences the pattern of ARH axonal projections involved in feeding regulation, we implanted the fluorescent axonal tracer DiI into the ARH of anti-ghrelin–treated neonates and control mice. Although the overall distribution of ARH DiI-labeled fibers was relatively similar between anti-ghrelin and control neonates, clear differences were apparent in the density of the labeled fibers. The density of DiI labeling in the PVH of P12 mice injected with anti-ghrelin was 1.5-fold higher than that observed in the control mice (Figure 4A). To determine whether the defect in ARH projections observed in the anti-ghrelin neonates was permanent, we performed immunohistochemical labeling of AgRP in brain sections from adult mice that were neonatally injected with the anti-ghrelin compound or the control. AgRP immunolabeling can be used as a marker of ARH projections because AgRP expression is restricted to the ARH in the adult mouse brain. The density of AgRP-IR fibers in the PVH was threefold higher in adult mice that were neonatally treated with anti-ghrelin compared with control mice (Figure 4B). In addition, the density of α-MSH-IR fibers (another neuropeptidergic system expressed by ARH neurons) innervating the PVH was twofold increased in adult mice neonatally treated with anti-ghrelin (Figure 4C). A substantial increase in the density of AgRP- and α-MSH–labeled fibers was observed in the parvocellular and magnocellular parts of the PVH (data not shown). Similar increases in AgRP and α-MSH fiber densities were also observed in the DMH and LHA (Supplemental Figure 1, A–D; supplemental material available online with this article; doi:10.1172/JCI73688DS1), which are other major terminal fields of ARH projections. These data indicate that neonatal ghrelin blockade causes the widespread disruption of ARH neural projections.

To address whether endogenous ghrelin controls hypothalamic development, we assessed ARH neural projections in ghrelin knockout (*Ghrl⁻/⁻*) mice (17). We detected significantly higher densities of DiI-labeled ARH axons in *Ghrl⁻/⁻* neonates compared with WT littermates at P12 and P21 (Figure 4, A and F). However, the density of DiI-labeled ARH axons in *Ghrl⁻/⁻* mice normalized at P35 (Figure 4F). Similarly, α-MSH– and AgRP-containing axons were normal in adult *Ghrl⁻/⁻* mice (Figure 4, B and C).

Many of the key events that occur during the development of functional neural systems, including the hypothalamus, are particularly sensitive to developmental cues during restricted ontogenic periods. These so-called critical periods tend to occur early in development and often coincide with the expression of signals that influ-

ence the formation of cellular nuclei and axonal connections. To test the structural effects of ghrelin in adults, we injected the anti-ghrelin compound from P100 to P107 and then evaluated AgRP and α-MSH fibers. In contrast to neonatal anti-ghrelin injections, adult injections with the anti-ghrelin did not affect the density of AgRP- and α-MSH-IR fibers (Figure 4, D and E, and Supplemental Figure 1, A–D). Consistent with these observations, adult anti-ghrelin injections do not cause marked metabolic alterations (Supplemental Figure 2). These results suggest that the neurodevelopmental activity of ghrelin is essentially restricted to the neonatal period.

Neonatal ghrelin blockade does not affect development of DMH projections. To determine whether neonatal ghrelin blockade also affected the development of other non-ARH circuits, we examined neuronal projections from the DMH, which is another hypothalamic nucleus known to contain high densities of ghrelin receptors (24). Despite a marked attenuation in the density of ARH DiI-labeled fibers, neural projections from the DMH appeared to be unaltered in anti-ghrelin–treated neonates (Supplemental Figure 3A), which suggests that neonatal ghrelin specifically affects the development of ARH projections. Consistent with these observations, ghrelin receptors were expressed at very low levels in the DMH throughout postnatal life. Notably, *Ghsr* mRNA levels were 4–5 times lower in the DMH compared with the ARH (Supplemental Figure 3B). Similarly, the number of ghrelin-induced pERK-IR cells was 4–5 times lower in the DMH compared with the ARH (Supplemental Figure 3C). Levels of *Ghsr* mRNA and ghrelin-induced pERK IR were also low in other hypothalamic and extrahypothalamic regions during neonatal life, suggesting that the developmental action of ghrelin might be primarily restricted to the ARH (Figure 1, G and H).

Ghrelin acts directly on ARH neurons to block axon growth. If ghrelin is a critical regulator of arcuate axon development, the direct exposure of ARH explants to ghrelin should result in changes in neurite outgrowth. To test the effects of ghrelin on neurite outgrowth, we incubated isolated ARH explants derived from P4 mice with ghrelin or vehicle. After 48 hours, the addition of ghrelin to the culture medium produced a twofold reduction in the density of neurites extending from ARH explants when compared with the control (Figure 5A). In addition to decreasing the density of ARH axons, ghrelin significantly reduced the overall length of axon extensions from ARH explants (Figure 5A). A substantial disruption of both AgRP and α-MSH fiber outgrowth was observed in ghrelin-treated explants (Supplemental Figure 1E). Together, these data provide direct evidence that ghrelin acts on ARH neurons to inhibit axonal growth and elongation. Notably, exposure of ARH explants to the anti-ghrelin compound prevented the ghrelin-induced decrease in neurite outgrowth (Figure 5B), further validating the use of the anti-ghrelin compound to inhibit ghrelin's action.

Neonatal hyperghrelinemia causes abnormal maturation of arcuate neural projections and metabolic disturbances. Our in vitro findings indicate that ghrelin inhibits ARH axon growth. On the basis of these observations, we next investigated whether a premature increase in ghrelin levels during neonatal life can impact hypothalamic development. Ghrelin was administered daily in WT pups from P4 to P12, i.e., when endogenous ghrelin levels are low (Figure 6A). Plasma levels of acylated ghrelin following exogenous i.p. ghrelin administration (2 mg/kg body weight) in neonates were markedly increased 15 minutes after injection, remained high 1 hour after
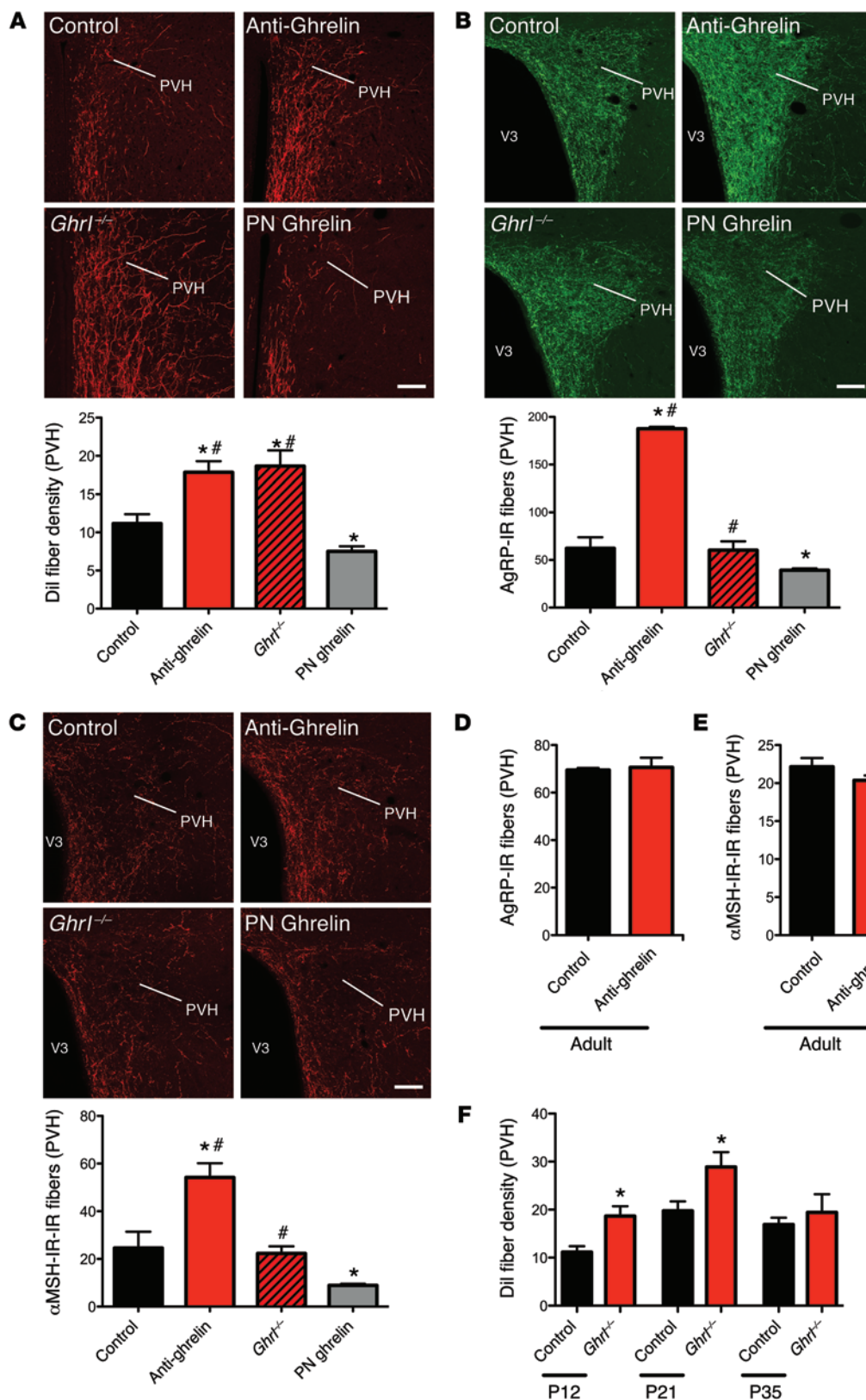
Figure 4. Neonatal ghrelin influences the normal developmental pattern of ARH neural projections. (**A**) Confocal images and quantification of the density of arcuate DiI-labeled fibers innervating the PVH in P12 mouse pups injected with the control, anti-ghrelin compound, or ghrelin, and ghrelin knockout ($Ghrl^{-/-}$) pups (n = 5 for control; n = 4 for $Ghrl^{-/-}$; n = 6 for anti-ghrelin and PN ghrelin). (**B** and **C**) Confocal images and quantification of AgRP-IR fibers (**B**) and α-MSH-IR fibers (**C**) at 100–120 days of age in the PVH of mice neonatally injected with the control or anti-ghrelin compound, mice neonatally injected with ghrelin, and $Ghrl^{-/-}$ mice (n = 6 for control, $Ghrl^{-/-}$, and PN ghrelin; n = 7 for anti-ghrelin). (**D** and **E**) Quantification of AgRP-IR (**D**) and α-MSH-IR (**E**) fibers at 100–120 days of age in the PVH of mice injected with control or anti-ghrelin during adult life (n = 3 per group). (**F**) Quantification of the density of arcuate DiI-labeled fibers innervating the PVH in P12, P21, and P35 control and ghrelin knockout ($Ghrl^{-/-}$) mice (n = 5 for control; n = 4 for P12 $Ghrl^{-/-}$; n = 6 for P21 and P35 $Ghrl^{-/-}$). Values are shown as the mean ± SEM. V3, third ventricle. *P < 0.05 vs. control; #P < 0.05 vs. PN ghrelin. Statistical significance was determined using 2-tailed Student's t tests (**D** and **E**) and a 2-way ANOVA followed by Bonferroni's post-hoc test (**A**, **B**, **C**, and **F**). Scale bars: 150 μm.

injection, and returned to levels similar to those in vehicle-treated pups by 12 hours after injection (Figure 6B). The density of ARH DiI-labeled fibers was 1.5-fold reduced in the PVH of P12 ghrelin-injected mice (postnatal [PN] ghrelin) as compared with control mice (Figure 4A). To determine whether the defects in ARH projections

observed in ghrelin-injected neonates were permanent, we also performed immunohistochemical labeling of AgRP and α-MSH in brain sections from adult mice that were neonatally injected with ghrelin or vehicle. Consistent with DiI labeling in neonates, the average density of AgRP-IR (Figure 4B) and α-MSH-IR (Figure 4C) fibers in
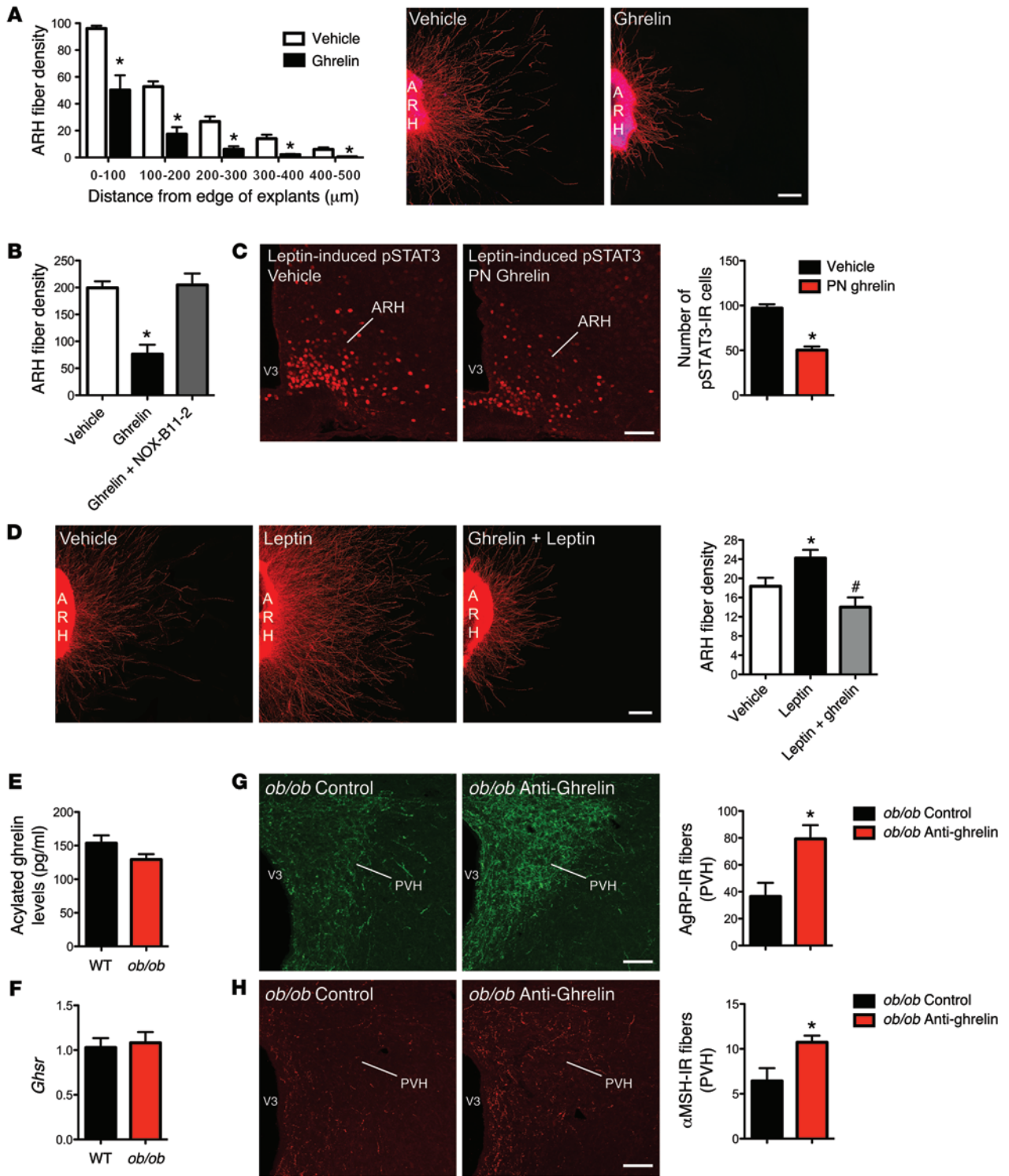
Figure 5. Ghrelin blocks axonal growth from neonatal ARH neurons. (**A**) Quantification and photomicrographs of βIII-tubulin–immunopositive fibers, a marker of neurites, from isolated organotypic cultures of neonatal ARH incubated for 48 hours with vehicle or ghrelin (100 ng/ml) (n = 6 cases per group). (**B**) Quantification of βIII-tubulin–immunopositive fibers from isolated cultures of neonatal ARH incubated for 48 hours with vehicle, ghrelin, or ghrelin and NOX-B11-2 (n = 8 for ghrelin, and ghrelin + NOX-B11-2; n = 11 for vehicle). (**C**) Photomicrographs and quantification of the number of leptin-induced pSTAT3-IR cells in the ARH of P10 pups injected with ghrelin (2 mg/kg) or vehicle from P4 to P10 (n = 4 for vehicle; n = 6 for PN ghrelin). (**D**) Images and quantification of the overall density of βIII-tubulin–immunopositive fibers from isolated organotypic cultures of neonatal ARH incubated for 48 hours with vehicle, leptin (100 ng/ml), or leptin + ghrelin (n = 9 for leptin; n = 15 for leptin + ghrelin; n = 19 for vehicle). (**E**) Circulating acylated ghrelin level of P10 WT and leptin-deficient (ob/ob) mice (n = 9 for WT; n = 12 for ob/ob). (**F**) Relative expression of Ghsr mRNA in the hypothalamus of P12 WT and ob/ob mice (n = 6 per group). (**G** and **H**) Confocal images and quantification of AgRP-IR fibers (**G**) and α-MSH-IR fibers (**H**) in the PVH of P12 ob/ob mice neonatally injected with the control or anti-ghrelin compound (n = 4 per group). Values are shown as the mean ± SEM. V3, third ventricle. *P < 0.05 vs. vehicle; #P < 0.05 vs. leptin. Statistical significance was determined using 2-tailed Student's t tests (**C** and **E**–**H**) and a 2-way ANOVA followed by Bonferroni's post-hoc test (**A**, **B**, and **D**). Scale bars: 100 μm (**A** and **D**); 150 μm (**C**, **G**, and **H**).
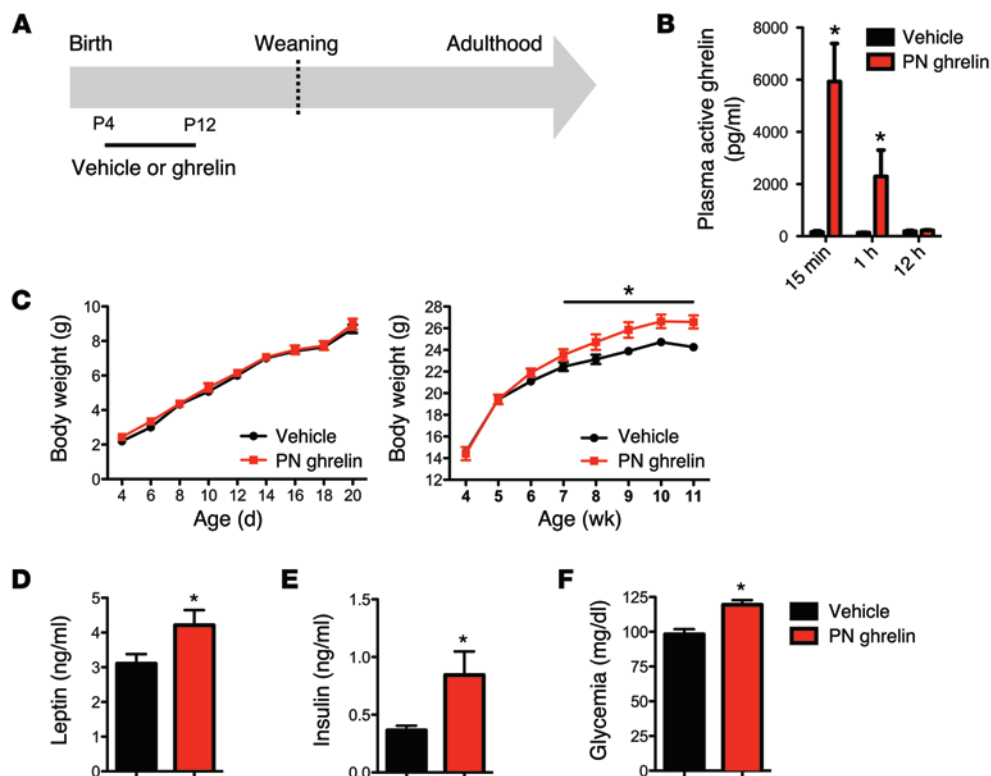
Figure 6. Chronic neonatal hyperghrelinemia causes metabolic disturbances. (**A**) Schematic representation of the experimental design used to increase ghrelin levels during neonatal life. Starting at P4, pups were treated daily with i.p. injections of ghrelin (2 mg/kg) (PN ghrelin) or vehicle (control), for a total of 8 days. (**B**) Acylated ghrelin levels in P10 mice injected with vehicle (0.9% NaCl) or ghrelin (2 mg/kg) (n = 4 for vehicle; n = 6 for PN ghrelin). Values are shown as the mean ± SEM. *P < 0.05 vs. control. (**C**) Pre- and postweaning growth curves (body weights) of mice neonatally injected with control or ghrelin (n = 5 for vehicle; n = 7 for PN ghrelin). (**D**) Plasma leptin and (**E**) insulin levels at 90 days of age in mice neonatally injected with control or ghrelin (n = 4 for control; n = 5 for PN ghrelin). (**F**) Fasting glucose levels in P80 mice neonatally injected with control or ghrelin (n = 5 for control; n = 7 for PN ghrelin). Values are shown as the mean ± SEM. *P < 0.05 vs. vehicle. Statistical significance was determined using 2-tailed Student's t tests (**D**–**F**) and a 2-way ANOVA followed by Bonferroni's post-hoc test (**B** and **C**).

the PVH was diminished in adult mice injected with ghrelin neonatally relative to that in control mice. However, α-MSH fibers were more markedly affected as compared with AgRP-IR fibers; mice injected with ghrelin neonatally had a 1.5- and 3-fold reduction of AgRP- and α-MSH-IR fibers, respectively, as compared with control mice (Figure 4, B and C). Consistent with previous studies indicating that a reduced density of AgRP- and α-MSH–containing fibers is associated with metabolic dysfunctions (6, 8, 13), adult animals neonatally injected with ghrelin also display metabolic disturbances (Figure 6, C–F). These results indicate that chronic neonatal hyperghrelinemia causes structural alterations in ARH neural circuits and long-term metabolic defects. However, the effect of neonatal ghrelin on body weight regulation appears sex specific, because treatment with the anti-ghrelin or ghrelin in neonatal female mice and rats, respectively, does not result in changes in body weight (data not shown and ref. 20).

Neonatal hyperghrelinemia attenuates leptin-induced pSTAT3 in the ARH. To better understand how a premature hyperghrelinemia during neonatal life can impair hypothalamic development, we conducted a series of studies to investigate the interaction between ghrelin and leptin signaling. The rationale for studying ghrelin-leptin interactions specifically is based on the observation that our ghrelin injection period coincides with a naturally occurring leptin surge that has been reported to promote ARH development (14). Because leptin's neurotrophic effects required intact ARH LepRb-pSTAT3 signaling (25), we first examined leptin-induced pSTAT3 in the ARH of neonates chronically injected with ghrelin. As expected, leptin treatment caused a marked increase in pSTAT3 staining in the ARH of control pups on P10 (Figure 5C). However, the same leptin treatment resulted in significantly fewer numbers of pSTAT3-IR cells in the ARH of P10 neonates chroni-

cally injected with ghrelin (Figure 5C). Ghrelin-injected neonates display a twofold reduction in pSTAT3-IR neurons following leptin administration as compared with control pups (Figure 5C). These results suggest that neonatal hyperghrelinemia impairs leptin signaling in ARH neurons during postnatal development in mice.

Ghrelin blunts the neurotrophic effect of leptin in vitro. Because neonates chronically injected with ghrelin exhibit impaired central leptin-induced pSTAT3 and because LepRb→pSTAT3 signaling is known to be critical for the regulation of ARH neurite outgrowth (25), we assessed whether alteration of projection pathways from the ARH in ghrelin-injected neonates could also be due to reduced ability of leptin to promote ARH neurite extension during development. As reported previously (14), organotypic ARH explants exposed to leptin (100 ng/ml) exhibit elevated ARH axon growth as compared with control, as revealed by a higher density of βIII-tubulin-IR fibers extending from the edge of ARH explants (Figure 5D). However, the neurotrophic effect of leptin on ARH axons was blunted when explants were also exposed to ghrelin (Figure 5D). Explants treated with both leptin and ghrelin had a 1.8-fold reduction of axons extending from the edge of ARH explants as compared with explants treated with leptin alone (Figure 5D). These in vitro data show that ghrelin blunts the trophic effect of leptin on ARH neurons.

Neonatal ghrelin blockade promotes development of ARH projections in ob/ob mice. Previous studies showed that ARH projections are markedly reduced in leptin-deficient (*ob/ob*) mice. Because neonatal ghrelin blockade increases the density of ARH fibers in WT mice, we next evaluated the ability of the anti-ghrelin compound to promote ARH projections in *ob/ob* mice. Circulating acylated ghrelin levels were comparable between WT and *ob/ob* mice at P10 (Figure 5E), and no differences were found in the hypothalamic *Ghsr* mRNA levels between WT and *ob/ob* pups (Figure 5F).

Neonatal injections of the anti-ghrelin compound from P4 to P12 resulted in a 2.2- and 1.7-fold increase in the density of AgRP- and αMSH-IR fibers, respectively (Figure 5, G and H).

Discussion

Ghrelin is one of the most potent orexigenic peptides identified so far. Both pharmacological and physiological evidence demonstrated that acute treatment of adult rats and mice with ghrelin stimulates food intake, increases body weight, and induces fat deposition (26–28). However, lifelong genetic deletion of ghrelin or its receptor results in normal growth and relatively unaltered food consumption, suggesting that lack of ghrelin during early life may cause compensatory developmental mechanisms (15–18). In the present study, we report that ghrelin exerts profound organizational effects on ARH neural projections during early postnatal life. We show that reduced ghrelin action results in enhanced densities of ARH neural projections during the preweaning period. In contrast, abnormally elevated levels of ghrelin permanently disrupt normal development of ARH neural projections.

Our data indicate that the ghrelin receptor Ghsr-1a is expressed at relatively high levels in the ARH as early as P6. The functionality of neonatal GHSRs is demonstrated by the ability of ghrelin to induce intracellular signaling (as evidenced by the induction of pERK IR). In adults, ghrelin acts primarily on NPY/AgRP neurons to regulate feeding (29, 30). Supporting these findings, the present study shows that, during neonatal life, ghrelin induces pERK IR in the vast majority of neonatal NPY/AgRP neurons, whereas only a small subset of POMC neurons exhibits pERK IR after ghrelin administration. Nevertheless, it is also known that ghrelin can also regulate the activity of POMC neurons indirectly, via trans-synaptic GABAergic inputs arising from NPY neurons (29, 31, 32). It is important to note that, during early postnatal life, GABA is not always an inhibitory transmitter but can also provide an excitatory drive (33). Consistent with the idea of an indirect effect of ghrelin on neonatal POMC neurons, treatment of P10 mice with ghrelin induces cFos expression in more than 25% of POMC neurons, whereas less than 6% of POMC neurons express pERK IR after ghrelin injections (data not shown). This observation is particularly interesting because cFos labels neurons that are both directly and trans-synaptically activated, whereas pERK is generally thought to be a marker of direct neuronal activation. These findings also raise the possibility that the change in POMC axon growth following ghrelin and anti-ghrelin treatment may be the result of non–cell-autonomous and/or post-synaptic mechanisms but also of cell-autonomous effects on a small portion of POMC neurons that express GHSR. Because the vast majority of NPY/AgRP neurons are known to express GHSR and respond to ghrelin directly, the regulation of axon growth in these neurons is likely to be cell autonomous. The exact nature of the effects of neonatal ghrelin on POMC and NPY neuronal activity also remains to be investigated. In adults, ghrelin depolarizes (activates) NPY/AgRP neurons whereas it hyperpolarizes (inhibits) POMC neurons. However, on the basis of our observations that NPY/AgRP and POMC projections are decreased in ghrelin-treated animals, it is likely that ghrelin exerts inhibitory effects on POMC but also on NPY/AgRP neurons during early postnatal life. Consistent with the idea that metabolic hormones can exert

different neurophysiological effects in neonates versus adults, a recent study from Baquero and colleagues reported that during the preweaning period leptin exerts stimulatory electrophysiological effects on NPY/AgRP neurons although it inhibits those same neurons at weaning and in adults (34). Notably, we found that ghrelin influences development of projections to both the neuroendocrine and preautonomic compartments of the PVH. The developmental action of ghrelin differs from that of leptin and insulin, which selectively promote formation of ARH projections to the preautonomic subdivision of the PVH (35, 36). However, like that of leptin, the developmental action of ghrelin appears to be primarily restricted to the ARH and does not affect projections originating from the DMH (the present study and ref. 14). It also remains possible that neonatal ghrelin could influence the development of nonfeeding circuits. Supporting this hypothesis, neonatal ghrelin injections perturb sexual maturation (20), suggesting that ghrelin can also influence the development of neuronal systems involved in reproductive function.

The precise mechanisms responsible for the disruption of ARH projections caused by ghrelin remain to be fully determined but likely involve an interaction with the well-documented trophic effect of leptin. In our animal model of chronic hyperghrelinemia, manipulation of ghrelin levels occurs when circulating ghrelin is physiologically low, i.e., from P4 to P12. Notably, this developmental window also coincides with a naturally occurring surge in circulating leptin that promotes formation of ARH projection pathways (14, 37). Whether there is a direct interaction between leptin and ghrelin signaling remains controversial. For example, although ARH neurons coexpress GHSR-1a and leptin receptors (38), GHSR knockout mice display unaltered leptin sensitivity (38). However, adult transgenic mice overexpressing ghrelin are resistant to the anorexigenic effects of leptin (39). Our data also support the hypothesis that ghrelin signaling can affect leptin sensitivity during neonatal life. Chronic hyperghrelinemia impairs the ability of neonatal leptin to induce phosphorylation of STAT3 in the ARH. Importantly, LepRb→pSTAT3 signaling is essential to mediate the neurotrophic effects of leptin on ARH neural projections (25). Our in vitro experiments further showed that ghrelin blunts the documented neurotrophic effect of leptin on ARH neurons. Remarkably, neonatal injection of anti-ghrelin also increases the density of POMC and AgRP projections in *ob/ob* mice, which display abnormal development of ARH projections (40). In contrast, neonatal leptin treatment in *ob/ob* mice only increases the density of AgRP fibers and has no effect on POMC-derived projections (35). This discrepancy suggests that the ability of ghrelin to modulate ARH axonal outgrowth is not exclusively dependent on leptin action.

The ultimate architecture of hypothalamic pathways involved in appetite regulation requires the precise temporal action of specific sets of hormones. A neonatal leptin surge (37) is followed by gradual increases in ghrelin levels (the present study and ref. 20), and these hormones appear to initiate and terminate the development of ARH neural projections, respectively. Previous studies reported that a premature, delayed, or abolished leptin surge causes disruption of ARH projections (41–43). In agreement with these findings, we found that advanced or blunted/delayed ghrelin action also alters ARH axon growth. These findings high-

light the importance of the correct timing of leptin and ghrelin actions to promote normal hypothalamic development. Like that of leptin, the developmental activity of ghrelin appears to be specific for ARH projections and is restricted to a neonatal window of maximum sensitivity that corresponds to a period when the ARH projections are established. Blockade of ghrelin during early postnatal life causes marked structural alterations; however, the treatment of adult mice with ghrelin does not affect the densities of ARH axons. Surprisingly, although ghrelin knockout neonates displayed a marked increase in the density of ARH projections, the density of both AgRP- and α-MSH–containing fibers became normal in adult ghrelin knockout mice. Our anatomical observations indicate that changes in ARH fiber projections in ghrelin knockout mice occur between P21 and P35. The precise biological substrates of these compensatory mechanisms remain to be investigated. Nevertheless, these data indicate that ARH peptidergic pathways continue to remodel and change not just early in development but even during the postweaning period in response to environmental influences as well as genetically programmed events. These data are also consistent with the "mismatch" hypothesis that suggests that when the pre- and postweaning environments are identical the phenotype is normal, whereas when there are changes in the environment between critical developmental periods and adult life, phenotypic aberrations develop (44). Our findings in adult animals are also in agreement with the absence of metabolic phenotype in ghrelin knockout mice.

Our results also indicate that not only the correct timing but also the correct amplitude of ghrelin is important for normal development of hypothalamic feeding pathways. Both a surfeit and a paucity of ghrelin action during early life cause alterations in hypothalamic development and long-term metabolic perturbations. A surprising finding was that abnormally high and low densities in ARH projections caused by the ghrelin and anti-ghrelin treatment, respectively, are associated with the same metabolic phenotype, i.e., elevated body weight and hyperglycemia. These findings are consistent with other neuroanatomical observations showing that both a reduction and an increase in neurogenesis and hypothalamic cell numbers are associated with obesity (45–48). These data indicate that appropriate patterns of hypothalamic connectivity must be established during development to accomplish an optimal control of energy metabolism and that both an excess and an insufficiency in hypothalamic feeding connections might affect the functionality of those circuits. The exact site of action of neonatal ghrelin to influence lifelong metabolic regulation remains to be determined; it likely involves a direct action at the level of the ARH. Consistent with the idea that intact hypothalamic projections are required for normal metabolic regulation, disruption of hypothalamic neural projections secondary to deletion of insulin signaling in POMC neurons is associated with impairment of glucose homeostasis (36). In addition, perturbations in the development of ARH projections are a common feature of animals subjected to metabolic programming (42, 43, 49, 50). Therefore, although future studies are needed to investigate the relative contribution of ARH neurons in the programming effects of neonatal ghrelin, it is likely that defective ARH projections contribute to the ultimate phenotype of mice treated with the anti-ghrelin and ghrelin. Nevertheless, it also remains possible

that neonatal ghrelin acts on peripheral organs that are known to express *Ghsr* mRNA during development, including the stomach, intestine, and pituitary gland (51).

In conclusion, our study defines a crucial organizational role for neonatal ghrelin during development and provides evidence for an interaction between multiple hormonal signals (leptin, ghrelin) to shape the ultimate architecture of hypothalamic feeding circuits. Our data also underline the importance of the correct magnitude and timing in ghrelin's action in influencing the development of ARH projection. These findings highlight the importance of timing for the design of optimal interventional studies to ameliorate diseases, such as metabolic syndrome. The physiopathological relevance of the present findings is supported by several observations. First, hyperghrelinemia is the hallmark of patients suffering from Prader-Willi syndrome (PWS). Remarkably, PWS patients exhibit a premature hyperghrelinemia that occurs before development of obesity and hyperphagia (52). Second, neonates exposed to undernutrition during intrauterine and/ or postnatal life display a marked increase in circulating ghrelin levels that is associated with higher risks of developing obesity and hyperphagia in later life (53). A better understanding of the relationship between neonatal ghrelin action and development of perinatally acquired metabolic diseases will be crucial as we seek to develop interventional studies to ameliorate and hopefully reverse this metabolic malprogramming.

Methods

Animals

C57BL/6 mice were housed in individual cages under specific-pathogen-free conditions, maintained in a temperature-controlled room with a 12-hour light/dark cycle, and provided *ad libitum* access to water and standard laboratory chow (Special Diet Services). Homozygous transgenic mice that selectively express EGFP in POMC-containing neurons and humanized renilla GFP (hrGFP) in NPY-containing neurons were provided by M. Low (Oregon Health & Science University, Portland, OR) and B. Lowell (Harvard Medical School, Boston, MA), respectively. For all experiments, the litter size was adjusted to 6 pups 1 day after birth to ensure adequate and standardized nutrition until weaning. Only male mice were studied.

Ghrelin knockout animals

Ghrl^{-/-} mice (on a C57BL/6 background) were obtained from Regeneron Pharmaceuticals and bred in the Monash Animal Services facility. This genetic mouse line has been described previously (17).

Ghrelin assays

Male offspring of C57BL/6 mice were decapitated on P6 ($n = 5$), P10 ($n = 5$), P14 ($n = 4$), and P90 (adult, $n = 6$), and trunk blood was collected in a chilled tube containing Pefabloc (AEBSF; Roche Diagnostics). Total and acylated ghrelin levels in the plasma were assayed using ELISA kits (Millipore). Acylated ghrelin levels were also characterized in mouse neonates injected with ghrelin. For this, P10 mice were injected with ghrelin (2 mg/kg) or vehicle (0.9% NaCl), and trunk blood was collected in a chilled tube containing Pefabloc (AEBSF; Roche Diagnostics) by decapitation 15 minutes, 1 hour, or 12 hours after injection ($n = 4$–6 per group).

For the fasting experiments, P6 and P14 mice were separated from their dams and placed on a heated pad for 4 hours before the experiment. Trunk blood was collected in a chilled tube containing Pefabloc (AEBSF; Roche Diagnostics), and acylated ghrelin levels in the plasma were assayed using ELISA kits (Millipore).

Measurement of *Ghsr* and *ghrelin* mRNA
ARH and DMH of P6, P10, P14, and P90 mice ($n = 4$–5 per group; for *Ghsr* analysis) and stomachs of P14 mice ($n = 7$ per group; for *ghrelin* analysis) fed *ad libitum* were dissected. Hypothalami of P12 *ob/ob* and WT littermates ($n = 6$ per group) fed *ad libitum* were also dissected. Total RNA was isolated using the Arcturus PicoPure RNA isolation kit (Invitrogen). cDNA was generated with the high-capacity cDNA Reverse Transcription Kit (Applied Biosystems). Quantitative real-time PCR analysis was performed using TaqMan Fast universal PCR Mastermix. mRNA expression was calculated using the 2-ddCt method after normalization with GAPDH as a housekeeping gene. Inventoried TaqMan gene expression assays *Ghsr* (Mm00616415_m1), *ghrelin* (Mm00445450_m1), and *Gapdh* (Mm99999915_g1) were used. All assays were performed using an Applied Biosystems StepOnePlus real-time PCR system.

pERK immunohistochemistry and analysis
On P6, P10, P14, or P90, WT mice were given an i.p. injection of ghrelin (2 mg/kg, $n = 4$–5 per group; Phoenix Pharmaceuticals) or vehicle alone (0.9% NaCl, $n = 4$ per group) and were perfused 45 minutes later with a solution of 4% PFA. POMC-EGFP and NPY-hrGFP mice were also injected with ghrelin or vehicle alone on P10 ($n = 4$–5 per group). Frozen coronal sections were cut at 20 μm and then processed for immunofluorescence. Briefly, sections were incubated for 48 hours in rabbit anti-pERK (1:1,000; Cell Signaling). The primary antibody was localized with Alexa Fluor 568 goat anti-rabbit IgGs (1:200; Invitrogen). Sections were then counterstained using bis-benzamide (1:10,000; Invitrogen) to visualize cell nuclei and coverslipped with buffered glycerol (pH 8.5).

Injections of the anti-ghrelin compound NOX-B11-2
Materials. Anti-ghrelin NOX-B11-2 and the nonfunctional control Spiegelmers were prepared by NOXXON Pharma AG, Berlin, as previously described (23).

Neonatal injections in WT mice. Offspring of C57BL/6 mice were used. Starting at P4, pups were treated daily with i.p. injections of NOX-B11-2 (15 mg/kg) or an inactive control (23) for a total of 18 days ($n = 8$–10 per group). To ensure identical development of the pups within the same litter, all pups of the same dam received administration of similar substances. Each experimental group in all experiments consisted of offspring from at least 3 litters.

Adult injections in WT mice. P100 mice were treated daily with i.p. injections of anti-ghrelin NOX-B11-2 (15 mg/kg) or an inactive control (23) for a total of 7 days ($n = 3$ per group).

Neonatal injections in ob/ob mice. Starting at P4, pups were treated daily with i.p. injections of NOX-B11-2 (15 mg/kg) or an inactive control for a total of 8 days ($n = 4$ per group).

Physiological measurements
Mice ($n = 8$–10 per group) were weighed every 2 days from P4 to P22 (weaning) and weekly after weaning using an analytical balance ($n = 8$–10 per group). The naso-anal length was also measured at weaning. To measure food consumption, mice were housed individually in cages, and,

after 1 week of acclimation, food intake was measured every 24 hours for 3 days from preweighed portions of food dispensed from the wire cage tops. The average daily food intake of each mouse ($n = 6$–8 per group) was used for statistical comparisons. MRI scanning (micro-MRI Bruker-Pharmascan 7T) was performed on mice fed *ad libitum* to evaluate in vivo body fat ($n = 3$–4 per group). Eighteen 0.75-mm-thick cross sections covering the whole abdominal cavity were acquired. Visceral, subcutaneous, and total fat was quantified using ITK-Snap 2.0.0 software (54). Fed glucose levels were assessed in adult mice ($n = 6$–8 per group) using a glucometer (One Touch Ultra; Johnson & Johnson). Glucose tolerance was performed in adult mice ($n = 12$ per group) by an i.p. administration of glucose (1.5 mg/g body weight) after overnight fasting, and then the blood glucose levels were measured 0, 15, 30, 45, 60, 90, 120, and 150 minutes after glucose challenge, as previously described (55). The leptin sensitivity test was performed in adult mice ($n = 5$ per group). Briefly, mice were injected i.p. at 6:30 pm with vehicle (5 mM sodium citrate buffer, pH 4.0) on day 1, followed by leptin on day 2 (1 mg/kg, PeproTech). Animals were weighed daily during the injection period. Serum leptin levels were assayed in the samples using a leptin ELISA kit (Millipore) ($n = 6$–8 per group).

Determination of stomach content in pups
The stomachs of P14 mice fed ad libitum ($n = 7$–8 per group) were rapidly dissected and weighed. They were then cut open, emptied of their contents, and weighed again. The difference between the full and empty stomach weight was used as an estimate of milk intake.

Neonatal ghrelin injections
Offspring of C57BL/6 mice were injected daily with ghrelin (2 mg/kg; Phoenix Pharmaceuticals) from P4 to P12. Controls received equivolume injections of vehicle (0.9% NaCl).

DiI implants
Mice ($n = 4$–6 per group) were perfused with 4% PFA. The brains were removed and numerically coded to ensure unbiased processing and analysis. Crystals of 1,1′-dioctadecyl-3,3,3′,3′-tetramethylindocarbocyanine perchlorate (DiI; Santa Cruz) were implanted as previously described (14). Briefly, an insect pin was used to place a crystal of DiI (15 μm in diameter) into the ARH of each brain under visual guidance. After incubation in the dark for 2 weeks at 37°C, hypothalamic sections were collected from each brain and evaluated by confocal microscopy as described below.

AgRP and α-MSH immunohistochemistry
Mice ($n = 3$–7 per group) were perfused transcardially with 4% PFA. The brains were then frozen and sectioned at a 30-μm thickness and processed for immunofluorescence using standard procedures (14). The primary antibodies used for IHC included rabbit anti-AgRP (1:4,000; Phoenix Pharmaceuticals) and sheep anti-α-MSH (1:40,000; Millipore). The primary antibodies were visualized with Alexa Fluor 488 goat anti-rabbit IgGs or Alexa Fluor 568 donkey anti-sheep IgGs (1:200; Invitrogen). Sections were counterstained using bis-benzamide (1:10,000; Invitrogen) to visualize cell nuclei and coverslipped with buffered glycerol (pH 8.5).

cFos immunohistochemistry
On P12, mice were injected i.p. with ghrelin (2 mg/kg; Phoenix Pharmaceuticals) or vehicle alone (0.9% NaCl) and perfused 2, 6, 12, or 24 hours later. Injections occurred 12 hours after the last injection of

anti-ghrelin or control solution. P21 and P36 mice neonatally injected with control or anti-ghrelin compound were also injected i.p. with ghrelin (2 mg/kg; Phoenix Pharmaceuticals) or vehicle alone (0.9% NaCl) and perfused 2 hours later. The brains were then frozen, sectioned at 25-μm thickness, and incubated in a rabbit primary antiserum directed against the N-terminal domain of Fos (1:2,000; Ab-5; Oncogene). The primary antibody was localized with affinity-purified IgGs conjugated with Alexa 488 (1:200; Invitrogen). Sections were counterstained using bis-benzamide (1:10,000) to visualize cell nuclei and coverslipped with buffered glycerol (pH 8.5).

pSTAT3 immunohistochemistry

Ghrelin (2 mg/kg; Phoenix Pharmaceuticals) was injected i.p. in pups daily from P4 to P9. Controls received equivolume injections of vehicle (0.9% NaCl). On P10, mice received an injection of ghrelin (2 mg/kg, i.p.), followed 2 days later by leptin administration (3 mg/kg, i.p.) (n = 4–6 per group). Animals were perfused 45 minutes later with a solution of 2% PFA. Frozen coronal sections were cut at 25 μm and pretreated for 20 minutes in 0.5% NaOH and 0.5% H_2O_2 in potassium PBS, followed by immersion in 0.3% glycine for 10 minutes. Sections were then placed in 0.03% SDS for 10 minutes and placed in 4% normal serum + 0.4% Triton X-100 + 1% BSA (fraction V) for 20 minutes before incubation for 48 hours with a rabbit anti-pSTAT3 antibody (1:1,000; Cell Signaling). The primary antibody was localized with Alexa Fluor 568 goat anti-rabbit IgGs (1:200; Invitrogen). Sections were counterstained using bis-benzamide (1:10,000; Invitrogen) to visualize cell nuclei, and coverslipped with buffered glycerol (pH 8.5).

Isolated ARH explant cultures

Brains were collected from P4 mice and sectioned at a 200-μm thickness with a vibroslicer as previously described (14). The ARH was then carefully dissected out of each section under a stereomicroscope. Explants (n = 6–19 cultures per group) were cultured onto a rat tail collagen matrix (BD Biosciences). Beginning on the first day in vitro, each explant was transferred to fresh modified Basal Medium Eagle (Invitrogen) containing either ghrelin (100 ng/ml; Phoenix Pharmaceuticals), leptin (100 ng/ml; PeproTech), leptin plus ghrelin (100 ng/ml each), or vehicle alone. To further validate the blocking effects of the anti-ghrelin compound on ghrelin's actions, ARH explants were also treated with ghrelin and NOX-B11-2 (100 ng/ml), or ghrelin and an inactive control (100 ng/ml). After 48 hours, the explants were fixed in PFA, and neurites extending from the explants were stained with βIII-tubulin (rabbit, 1:5,000; Covance) as described previously (56).

Quantitative analysis of cell numbers and fiber density

For the histological experiments, 2 sections through the ARH (for pERK and pSTAT3 staining) and the PVH, DMH, and LHA (for α-MSH and AgRP staining and DiI labeling) from animals of each experimental group (n = 3–7 animals per group) were acquired using a Zeiss LSM 710 confocal system equipped with a ×20 objective. For the in vitro

experiments, sections through 5 different regions of interest (100 × 100 μm) spaced at 100, 200, 300, 400, and 500 μm extending radially from the edge of the ARH explants (n = 6–19 per group) were acquired using a Zeiss LSM 710 confocal system equipped with a ×10 objective. Slides were numerically coded to obscure the treatment group. Image analysis was performed using ImageJ analysis software (NIH).

For the quantitative analysis of fiber density (for α-MSH, AgRP, and DiI), each image plane was binarized to isolate labeled fibers from the background and to compensate for differences in fluorescence intensity. The integrated intensity, which reflects the total number of pixels in the binarized image, was then calculated for each image. This procedure was conducted for each image plane in the stack, and the values for all of the image planes in a stack were summed. The resulting value is an accurate index of the density of the processes in the volume sampled (14).

For the quantitative analysis of cell number, the numbers of pERK-, pSTAT3-, POMC-, NPY-, POMC+pERK-, and NPY+pERK-labeled cells in the ARH were manually counted using ImageJ analysis software (NIH). Only GFP-positive cells that had a corresponding bis-benzamide–stained nucleus were included in our counts. The average number of cells counted in 2 ARH hemisections from each mouse was used for statistical comparisons.

Statistics

All values were expressed as the means ± SEM. Statistical analyses were conducted using GraphPad Prism (version 5.0a). Statistical significance was determined using unpaired 2-tailed Student's t tests and a 2-way ANOVA followed by the Bonferroni post hoc test when appropriate. $P < 0.05$ was considered to be statistically significant.

Study approval

Animal usage was in compliance with and approved by the Institutional Animal Care and Use Committee of the Saban Research Institute of Children's Hospital Los Angeles.

Address correspondence to: Sebastien G. Bouret, The Saban Research Institute, Developmental Neuroscience Program, Children's Hospital Los Angeles, University of Southern California, 4650 Sunset Boulevard, MS#135, Los Angeles, California 90027, USA. Phone: 323.361.8743; E-mail: sbouret@chla.usc.edu.

1. Elmquist JK, Maratos-Flier E, Saper CB, Flier JS. Unraveling the central nervous system pathways underlying responses to leptin. *Nat Neurosci*. 1998;1(6):445–450.
2. Nogueiras R, Tschoep MH, Zigman JM. Central nervous system regulation of energy metabo-

lism: ghrelin versus leptin. *Ann N Y Acad Sci*. 2008;1126:14–19.
3. Zhang Y, Proenca R, Maffel M, Barone M, Leopold L, Friedman JM. Position cloning of the mouse obese gene and its human homologue. *Nature*. 1994;372(6505):425.

4. Kojima M, Hosoda H, Date Y, Nakazato M, Matsuo H, Kangawa K. Ghrelin is a growth-hormone-releasing acylated peptide from stomach. *Nature*. 1999;402(6762):656–660.
5. Nakazato M, et al. A role for ghrelin in the central regulation of feeding. *Nature*.

2001;409(6817):194–198.

6. Levin BE. The obesity epidemic: metabolic imprinting on genetically susceptible neural circuits. *Obes Res*. 2000;8(4):342–347.

7. Martin-Gronert MS, Ozanne SE. Programming of appetite and type 2 diabetes. *Early Hum Dev*. 2005;81(12):981–988.

8. Sullivan EL, Grove KL. Metabolic imprinting in obesity. *Forum Nutr*. 2010;63:186–194.

9. Dickson SL. Ghrelin: a newly discovered hormone. *J Neuroendocrinol*. 2002;14(1):83–84.

10. Elmquist JK, Coppari R, Balthasar N, Ichinose M, Lowell BB. Identifying hypothalamic pathways controlling food intake, body weight, and glucose homeostasis. *J Comp Neurol*. 2005;493(1):63–71.

11. Williams KW, Elmquist JK. From neuroanatomy to behavior: central integration of peripheral signals regulating feeding behavior. *Nat Neurosci*. 2012;15(10):1350–1355.

12. Gao Q, Horvath TL. Neurobiology of feeding and energy expenditure. *Annu Rev Neurosci*. 2007;30:367–398.

13. Bouret SG. Development of hypothalamic neural networks controlling appetite. In: Elmadfa I, ed. *Forum Nutr*. Basel, Switzerland: Karger; 2010:84–93.

14. Bouret SG, Draper SJ, Simerly RB. Trophic action of leptin on hypothalamic neurons that regulate feeding. *Science*. 2004;304(5667):108–110.

15. Sun Y, Ahmed S, Smith RG. Deletion of ghrelin impairs neither growth nor appetite. *Mol Cell Biol*. 2003;23(22):7973–7981.

16. Sun Y, Wang P, Zheng H, Smith RG. Ghrelin stimulation of growth hormone release and appetite is mediated through the growth hormone secretagogue receptor. *Proc Natl Acad Sci U S A*. 2004;101(13):4679–4684.

17. Wortley KE, et al. Genetic deletion of ghrelin does not decrease food intake but influences metabolic fuel preference. *Proc Natl Acad Sci U S A*. 2004;101(21):8227–8232.

18. Zigman JM, et al. Mice lacking ghrelin receptors resist the development of diet-induced obesity. *J Clin Invest*. 2005;115(12):3564–3572.

19. Grove KL, Cowley MA. Is ghrelin a signal for the development of metabolic systems? *J Clin Invest*. 2005;115(12):3393–3397.

20. Hayashida T, et al. Ghrelin in neonatal rats: distribution in stomach and its possible role. *J Endocrinol*. 2002;173(2):239–245.

21. Holst B, Holliday ND, Bach A, Elling CE, Cox HM, Schwartz TW. Common structural basis for constitutive activity of the ghrelin receptor family. *J Biol Chem*. 2004;279(51):53806–53817.

22. Helmling S, et al. Inhibition of ghrelin action in vitro and in vivo by an RNA-Spiegelmer. *Proc Natl Acad Sci U S A*. 2004;101(36):13174–13179.

23. Shearman LP, et al. Ghrelin neutralization by a ribonucleic acid-SPM ameliorates obesity in diet-induced obese mice. *Endocrinology*. 2006;147(3):1517–1526.

24. Zigman JM, ones JE, Lee CE, Saper CB, Elmquist JK. Expression of ghrelin receptor mRNA in the rat and the mouse brain. *J Comp Neurol*. 2006;494(3):528–548.

25. Bouret SG, Bates SH, Chen S, Myers MG, Simerly RB. Distinct roles for specific leptin receptor signals in the development of hypothalamic feeding circuits. *J Neurosci*. 2012;32(4):1244–1252.

26. Tschöp M, Smiley DL, Heiman ML. Ghrelin induces adiposity in rodents. *Nature*. 2000;407(6806):908–913.

27. Nakazato M, et al. A role for ghrelin in the central regulation of feeding. *Nature*. 2001;409(6817):194–198.

28. Chen HY, et al. Orexigenic action of peripheral ghrelin is mediated by neuropeptide Y and agouti-related protein. *Endocrinology*. 2004;145(6):2607–2612.

29. Cowley MA, et al. The distribution and mechanism of action of ghrelin in the CNS demonstrates a novel hypothalamic circuits regulating energy homeostasis. *Neuron*. 2003;37(4):649–661.

30. Willesen MG, Kristensen P, Rømer J. Co-localization of growth hormone secretagogue receptor and NPY mRNA in the arcuate nucleus of the rat. *Neuroendocrinology*. 1999;70(5):306–316.

31. Tong Q, Ye C-P, Jones JE, Elmquist JK, Lowell BB. Synaptic release of GABA by AgRP neurons is required for normal regulation of energy balance. *Nat Neurosci*. 2008;11(9):998–1000.

32. Andrews ZB, et al. UCP2 mediates ghrelin's action on NPY/AgRP neurons by lowering free radicals. *Nature*. 2008;454(7206):846–851.

33. Cherubini E, Gaiarsa JL, Ben-Ari Y. GABA: an excitatory transmitter in early postnatal life. *Trends Neurosci*. 1991;14(12):515–519.

34. Baquero AF, et al. Developmental switch of leptin signaling in arcuate nucleus neurons. *J Neurosci*. 2014;34(30):9982–9994.

35. Bouyer K, Simerly RB. Neonatal leptin exposure specifies innervation of presympathetic hypothalamic neurons and improves the metabolic status of leptin-deficient mice. *J Neurosci*. 2013;33(2):840–851.

36. Vogt MC, et al. Neonatal insulin action impairs hypothalamic neurocircuit formation in response to maternal high-fat feeding. *Cell*. 2014;156(3):495–509.

37. Ahima R, Prabakaran D, Flier J. Postnatal leptin surge and regulation of circadian rhythm of leptin by feeding. Implications for energy homeostasis and neuroendocrine function. *J Clin Invest*. 1998;101(5):1020–1027.

38. Perello M, et al. Functional implications of limited leptin receptor and ghrelin receptor coexpression in the brain. *J Comp Neurol*. 2012;520(2):281–294.

39. Bewick GA, Kent A, Campbell D. Mice with hyperghrelinemia are hyperphagic and glucose intolerant and have reduced leptin sensitivity. *Diabetes*. 2009;58(4):840–846.

40. Bouret SG, et al. Leptin promotes formation of projection pathways from the arcuate nucleus of the hypothalamus through activation of ObRb signaling pathways. Presented at: Proceedings of the 34th Annual Meeting The Society For Neuroscience; October 23–27, 2004; San Diego, California, USA.

41. Attig L, et al. Early postnatal leptin blockage leads to a long-term leptin resistance and susceptibility to diet-induced obesity in rats. *Int J Obes*. 2008;32(7):1153–1160.

42. Kirk SL, et al. Maternal obesity induced by diet in rats permanently influences central processes regulating food intake in offspring. *PLoS One*. 2009;4(6):e5870.

43. Delahaye F, et al. Maternal perinatal undernutrition drastically reduces postnatal leptin surge and affects the development of arcuate nucleus proopiomelanocortin neurons in neonatal male rat pups. *Endocrinology*. 2008;149(2):470–475.

44. Bateson P, Gluckman P, Hanson M. The biology of developmental plasticity and the Predictive Adaptive Response hypothesis. *J Physiol*. 2014;592(pt 11):2357–2368.

45. Chang G-Q, Gaysinskaya V, Karatayev O, Leibowitz SF. Maternal high-fat diet and fetal programming: increased proliferation of hypothalamic peptide-producing neurons that increase risk for overeating and obesity. *J Neurosci*. 2008;28(46):12107–12119.

46. Sousa-Ferreira L, de Almeida LP, Cavadas C. Role of hypothalamic neurogenesis in feeding regulation. *Trends Endocrinol Metab*. 2014;25(2):80–88.

47. McNay DEG, on N, Kokoeva MV, Maratos-Flier E, Flier JS. Remodeling of the arcuate nucleus energy-balance circuit is inhibited in obese mice. *J Clin Invest*. 2012;122(1):142–152.

48. Kokoeva MV, Yin H, Flier JS. Neurogenesis in the hypothalamus of adult mice: potential role in energy balance. *Science*. 2005;310(5748):679–683.

49. Coupe B, Amarger V, Grit I, Benani A, Parnet P. Nutritional programming affects hypothalamic organization and early response to leptin. *Endocrinology*. 2010;151(2):702–713.

50. Schipper L, Bouyer K, Oosting A, Simerly RB, van der Beek EM. Postnatal dietary fatty acid composition permanently affects the structure of hypothalamic pathways controlling energy balance in mice. *Am J Clin Nutr*. 2013;98(6):1395–1401.

51. Nakahara K, et al. Maternal ghrelin plays an important role in rat fetal development during pregnancy. *Endocrinology*. 2006;147(3):1333–1342.

52. Feigerlová E, et al. Hyperghrelinemia precedes obesity in Prader-Willi syndrome. *J Clin Endocrinol Metab*. 2008;93(7):2800–28005.

53. Desai M, Gayle D, Babu J, Ross MG. Programmed obesity in intrauterine growth-restricted newborns: modulation by newborn nutrition. *Am J Physiol Regul Integr Comp Physiol*. 2005;288(1):R91–R96.

54. Yushkevich PA, et al. User-guided 3D active contour segmentation of anatomical structures: Significantly improved efficiency and reliability. *NeuroImage*. 2006;31(3):1116–1128.

55. Coupe B, Ishii Y, Dietrich MO, Komatsu M, Horvath TL, Bouret SG. Loss of autophagy in proopiomelanocortin neurons perturbs axon growth and causes metabolic dysregulation. *Cell Metab*. 2012;15(2):247–255.

56. Bouret SG, Gorski JN, Patterson CM, Chen S, Levin BE, Simerly RB. Hypothalamic neural projections are permanently disrupted in diet-induced obese rats. *Cell Metab*. 2008;7(2):179–185.